A Model for Extremely Heterogeneous Clutter

Alejandro César Frery, *Member, IEEE*, Häns-Jürgen Müller, Corina da Costa Freitas Yanasse, and Sidnei João Siqueira Sant'Anna

***Abstract*—A new class of distributions, $\mathcal{G}$ distributions, arising from the multiplicative model is presented in this paper, along with their main properties and relations. Their densities are derived for complex and multilook intensity and amplitude data. Classical distributions, such as $\mathcal{K}$, are particular cases of this new class. A special case of this class called here $\mathcal{G}^0$, that has as many parameters as $\mathcal{K}$ distributions, is shown able to model extremely heterogeneous clutter, such as that of urban areas, that cannot be properly modeled with $\mathcal{K}$ distributions. One of the parameters of this special case is related to the degree of homogeneity, and a limiting case is that of a scaled speckle. The advantage of the $\mathcal{G}^0$ distribution becomes evident through the analysis of a variety of areas (urban, primary forest and deforested) from two sensors.**

I. Introduction

THE PRECISE knowledge of the statistical properties of SAR data plays a central role in image processing and understanding. These properties can be used to discriminate types of land use and to develop specialized filters for speckle noise reduction, among other applications. Several studies have been conducted in order to relate physical features and statistical properties of SAR data and, in order to do this, some hypothesis and distributions are considered.

The multiplicative model has been widely used in the modeling, processing, and analysis of synthetic aperture radar images. This model states that, under certain conditions [15], the return results from the product between the speckle noise and the terrain backscatter. Several distributions could be used for the backscatter, aiming at the modeling of different types of classes and their characteristic degrees of homogeneity. For instance, for some sensor parameters (wavelength, angle of incidence, polarization, etc.), pasture is more homogeneous than forest, which, in turn, is more homogeneous than urban areas. Most distributions for the (amplitude) backscatter do not yield to closed-form distributions for the return, being a constant, a square root of Gamma and a square root of generalized inverse Gaussian distribution important exceptions.

Common distributional hypothesis for one-look return data and homogeneous targets are the Exponential and Rayleigh distributions, for quadratic and linear detections, respectively. When the observed region cannot be assumed as homogeneous, other distributions are considered. Among these, the $\mathcal{K}$ distributions have received a great deal of attention in the literature [8], [9], [13], [14].

This paper extends classical results with the proposal of distributions that have the $\mathcal{K}$ distributions as particular cases. These distributions arise using the square root of generalized inverse Gaussian distribution as the model for the amplitude backscatter, a distribution here proposed to model extremely heterogeneous targets as well as other types of clutter.

This work is organized in the following manner: complex and amplitude cases for the speckle noise are treated separately; distributions that model the terrain backscatter (amplitude case) are then reviewed, and the square root of the generalized inverse Gaussian distribution is introduced. Once the speckle noise and the backscatter are characterized, attention is devoted to the distributions induced for the return. It is shown that a two-parameters particular case of the square root of generalized inverse Gaussian distribution can be succesfully used as a model for urban areas backscatter, a problem addressed by several authors (see [12] and [16]). The distribution induced for the return, called here $\mathcal{G}^0$, is also used to model primary forests and a deforested area.

II. The Multiplicative Model and the Speckle Noise

Speckle noise is always associated to coherent-illuminated scenes, such as those obtained by microwaves, laser, ultrasonography, etc. This kind of noise appears due to interference phenomena between the incident and reflected signals. This kind of noise makes visual and automatic interpretation a difficult task, though it may carry important information. As will be seen in this section, images suffering from speckle noise should not be treated with the usual additive-noise derived tools (Wiener filter, for instance), since speckle corrupts the signal in a multiplicative manner and in the amplitude and intensity formats it is non-Gaussian.

The multiplicative model is a common framework used to explain the statistical behavior of data obtained with coherent illumination. It assumes that the observations within this kind of images are the outcome of the product of two independent random variables: one (X) modeling the terrain backscatter, and other (Y) modeling the speckle noise. The former is many times considered real and positive, while the latter could be complex (if the considered image is in complex format) or positive real (intensity and amplitude formats).

Therefore, the observed value is the outcome of the random variable defined by the product $Z = X \cdot Y$. In order to make a clear distinction between the aforementioned formats, the

Manuscript received November 13, 1995; revised September 10, 1996. This work was supported by FAPESP (Project 91/3532-2), PROTEM-CC/CNPq, and Process 680.061-94-0 (GEOTEC Project).

A. C. Frery is with the Departamento de Informática, Universidade Federal de Pernambuco, 50732 Recife, PE-Brazil (e-mail: frery@di.ufpe.br).

H.-J. Müller is with Deutsche Forschungsanstalt für Luft-und Raumfahrt, Institut für Hochfrequenztechnik, D-82230 Weßling, Germany (e-mail: hj.mueller@dlr.de).

C. C. F. Yanasse and S. J. S. Sant'Anna are with the Instituto Nacional de Pesquisas Espaciais, Divisão de Processamento de Imagens, 12227 São José dos Campos, SP-Brazil (e-mails: corina@dpi.inpe.br; sidnei@dpi.inpe.br).

Publisher Item Identifier S 0196-2892(97)02103-7.

subscripts "C," "I," and "A" will be used for the complex, intensity, and amplitude cases, respectively. Vectors will be explicitly denoted in boldface.

Complex speckle is usually assumed to have a bivariate normal distribution, with independent identically distributed components having zero mean and variance $1/2$. These marginal distributions are denoted here as $\mathcal{N}(0,1/2)$; therefore, $\mathbf{Y}_C = (Y_\Re, Y_\Im) \sim \mathcal{N}2(\mathbf{0}, \mathbf{1/2})$ denotes the distribution of the pair.

Multilook intensity speckle appears by taking the average over n independent samples of $Y_I = ||\mathbf{Y}_C||^2$ leading, thus, to a Gamma distribution denoted here as $Y_I \sim \Gamma(n,n)$ and characterized by the density

$$f_{Y_I}(y) = \frac{n^n}{\Gamma(n)} y^{n-1} \exp(-ny), \quad y, n > 0.$$

Multilook amplitude speckle results from taking the square root of the multilook intensity speckle and, therefore, has a square root of Gamma distribution, denoted here as $Y_A \sim \Gamma^{1/2}(n,n)$ and characterized by the density

$$f_{Y_A}(y) = \frac{2n^n}{\Gamma(n)} y^{2n-1} \exp(-ny^2), \quad y, n > 0.$$

Though the number of looks n should, in principle, be an integer, seldom this is the case when this quantity is estimated from real data due to, among other reasons, the fact that the mean is taken over correlated observations. It is therefore interesting to call n the *equivalent* number of looks; its estimation is discussed in [17] and [18].

III. Amplitude Backscatter

Two models are found in the literature for the amplitude backscatter within the multiplicative model: a constant (used to model homogeneous areas) and a square root of Gamma distribution (used to model heterogeneous areas), being the former a particular case of the latter. In Section V it will be seen that these distributions lead to the square root of Gamma and to the amplitude $\mathcal{K}$ distributions for the amplitude return, respectively. In [12] and [16], it was noticed that the observations from some areas were heterogeneous to an extent that even $\mathcal{K}$ distributions could not take account of.

In this paper the use of the square root of a generalized inverse Gaussian distribution is proposed as a general model for the amplitude backscatter which

- yields to closed form densities for the complex, intensity and amplitude returns under the multiplicative model with Gaussian complex speckle;
- has the following distributions as particular cases:
  - — the square root of Gamma, leading to the class of $\mathcal{K}$ distributions for the return;
  - — the reciprocal of a square root of Gamma, leading to the class of $\mathcal{G}^0$ distributions for the return;
  - — a constant, leading to scaled speckle for the return.
- The class of $\mathcal{G}^0$ distributions has as many parameters as the $\mathcal{K}$ distributions, and allows the modeling of extremely heterogeneous areas (as is the case of urban data), as well as other types of areas.

The amplitude backscatter is said to obey the square root of generalized inverse Gaussian law, situation here denoted as $X_A \sim \mathcal{N}^{-1/2}(\alpha, \gamma, \lambda)$, if its density is given by

$$f_{X_A}(x) = \frac{(\lambda/\gamma)^{\alpha/2}}{K_\alpha(2\sqrt{\lambda\gamma})} x^{2\alpha-1} \exp\left(-\frac{\gamma}{x^2} - \lambda x^2\right), \quad x > 0$$

where K_α denotes the modified Bessel function of the third kind and order α, and the parameters space is given by

$$\begin{cases} \gamma > 0, & \lambda \geq 0 \quad \text{if } \alpha < 0 \\ \gamma > 0, & \lambda > 0 \quad \text{if } \alpha = 0. \\ \gamma \geq 0, & \lambda > 0 \quad \text{if } \alpha > 0 \end{cases} \tag{1}$$

Its r-th order moments are given by

$$E(X_A^r) = \left(\frac{\gamma}{\lambda}\right)^{r/4} \frac{K_{\alpha+r/2}(2\sqrt{\gamma\lambda})}{K_\alpha(2\sqrt{\gamma\lambda})}.$$

If $X_A \sim \mathcal{N}^{-1/2}(\alpha, \gamma, \lambda)$, then the intensity basckscatter $X_I = X_A^2$ is said to have the generalized inverse Gaussian distribution. An extensive account of properties and applications of this last distribution can be seen in [1], [10].

Two particular cases of this distribution are of interest in SAR data analysis: the square root of Gamma, and the reciprocal of a square root of Gamma distributions. The former is a well known model for homogeneous and heterogeneous clutter. The latter is a proposal of this paper that encompasses the modeling abilities of the former whilst extending them to enable the modeling of more heterogeneous (*extremely* heterogeneous) data. This new model was motivated by statistical fitting of areas with varying degrees of homogeneity [3], [4], [18], [19].

The square root of Gamma distribution arises by letting $\gamma \to 0$ while $\alpha, \lambda > 0$. This distribution, denoted here as $\Gamma^{1/2}(\alpha, \lambda)$ is characterized by the density

$$f_{X_A}(x) = \frac{2\lambda^\alpha}{\Gamma(\alpha)} x^{2\alpha-1} \exp(-\lambda x^2), \quad \alpha, \lambda, x > 0. \tag{2}$$

Square root of Gamma distributed backscatter is a commonly used model for heterogeneous areas, as is the case of forests for some SAR sensors. This hypothesis is mainly based on empirical evidence, though some theoretical results relating backscatter with birth-and-death processes can be found in [2].

The reciprocal of the square root of Gamma distribution arises by letting $\lambda \to 0$ while $-\alpha, \gamma > 0$. This distribution, denoted here as $\Gamma^{-1/2}(\alpha, \gamma)$ is characterized by the density

$$f_{X_A}(x) = \frac{2}{\gamma^\alpha \Gamma(-\alpha)} x^{2\alpha-1} \exp(-\gamma/x^2), \quad -\alpha, \gamma, x > 0. \tag{3}$$

Notice that, if $X'_A \sim \Gamma^{1/2}(\eta, \gamma)$, then (3) characterizes the distribution of $X_A = 1/X'_A$ with $\alpha = -\eta$.

Using characteristic functions it can be proved that a sequence of random variables obeying $\Gamma^{1/2}(\alpha_m, \lambda_m)$ distributions converges in probability to the constant $\beta_1^{1/2}$, if $\alpha_m, \lambda_m \to \infty$ such that $\alpha_m/\lambda_m \to \beta_1$ when $m \to \infty$. Also, a sequence of random variables obeying $\Gamma^{-1/2}(\alpha_m, \gamma_m)$ distributions converges in probability to the constant $\beta_2^{-1/2}$, if $-\alpha_m, \gamma_m \to \infty$ such that $-\alpha_m/\gamma_m \to \beta_2$ when $m \to \infty$. In this manner, constant amplitude backscatter, used to model

homogeneous areas, arises in two situations ($\beta_1^{1/2}$ and $\beta_2^{-1/2}$) as particular cases of the square root of generalized inverse Gaussian distribution.

The aforementioned limiting properties that relate the $\mathcal{N}^{-1/2}(\alpha,\gamma,\lambda)$ distribution with $\Gamma^{1/2}(\alpha,\lambda)$, $\Gamma^{-1/2}(\alpha,\gamma)$ and constants are summarized in (4), where "$\xrightarrow{\mathcal{D}}$" and "$\xrightarrow{\Pr}$" denote the convergences in distribution and probability, respectively, of the associated random variables. The properties stated in relations (4), shown at the bottom of the page, show that either homogeneous, heterogeneous, or extremely heterogeneous backscatters can be treated as the outcome of a $X_A \sim \mathcal{N}^{-1/2}(\alpha,\gamma,\lambda)$ random variable.

IV. Complex Return

Once defined the general distribution for X_A as being $\mathcal{N}^{-1/2}(\alpha,\gamma,\lambda)$, and given that the complex speckle is assumed to be $\mathbf{Y}_C = (Y_\Re, Y_\Im) \sim \mathcal{N}2(\mathbf{0},\mathbf{1/2})$ distributed, it is possible to derive the associated marginal distribution for the complex return, which is given by $\mathbf{Z}_C = X_A \cdot \mathbf{Y}_C = X_A \cdot (Y_\Re, Y_\Im)$. The density that characterizes the distribution of either the real or imaginary part of $\mathbf{Z}_C$, denoted by $Z_\circ$, is given by

$$f_{Z_\circ}(x) = \frac{1}{K_\alpha(2\sqrt{\lambda\gamma})}\sqrt{\frac{(\lambda/\gamma)^\alpha}{\pi}}\left(\frac{\gamma+x^2}{\lambda}\right)^{(\alpha-1/2)/2} \times K_{\alpha-1/2}(2\sqrt{\lambda(\gamma+x^2)}), \quad x \in \mathbb{R},$$

and parameter space given in (1). This distribution is denoted here as $\mathcal{G}_C(\alpha,\gamma,\lambda)$, and its r-th order moments are given by

$$E(Z_\circ^r) = \begin{cases} 0 & \text{if } r \text{ is odd} \\ \frac{K_{\alpha+r/2}(2\sqrt{\gamma\lambda})}{K_\alpha(2\sqrt{\gamma\lambda})}\left(\frac{\gamma}{4\lambda}\right)^{r/4}(1\cdot 3\cdot\cdots\cdot(r-1)) & \text{else.} \end{cases}$$

The relations presented in (4) yield to the properties for the marginal return presented in (5), shown at the bottom of the page, where $\mathcal{K}_C(\alpha,\lambda)$ and $\mathcal{G}_C^0(\alpha,\lambda)$ denote the complex $\mathcal{K}$ and $\mathcal{G}^0$ distributions, respectively, characterized by the densities

$$f_{Z_\circ}(x) = \frac{2}{\Gamma(\alpha)}\sqrt{\frac{\lambda^{\alpha+1/2}}{\pi}}|x|^{\alpha-1/2}K_{\alpha-1/2}(2|x|\sqrt{\lambda}), \quad \alpha,\lambda>0,\ x\in\mathbb{R},$$

$$f_{Z_\circ}(x) = \frac{\Gamma(1/2-\alpha)}{\sqrt{\pi}\gamma^\alpha\Gamma(-\alpha)}(x^2+\gamma)^{\alpha-1/2}, \quad -\alpha,\gamma>0,\ x\in\mathbb{R}.$$

These distributions have rth order moments given, respectively, by

$$\mathrm{E}(Z_\circ^r) = \begin{cases} 0 & \text{if } r \text{ is odd} \\ \frac{\Gamma(-\alpha-r/2)(\gamma/2)^{r/2}}{\Gamma(-\alpha)}(1\cdot 3\cdot\cdots\cdot(r-1)) & \text{else.} \end{cases}$$

$$E(Z_\circ^r) = \begin{cases} 0 & \text{if } r \text{ is odd} \\ \frac{\Gamma(\alpha+r/2)}{(2\lambda)^{r/2}\Gamma(\alpha)}(1\cdot 3\cdot\cdots\cdot(r-1)) & \text{else.} \end{cases}$$

Using the parametrization presented here, it can be easily checked that the $\mathcal{G}_C$ distribution is a particular case of the generalized hyperbolic distribution. It is interesting to note that the generalized hyperbolic distribution (see [1] for its properties and applications) is defined for an arbitrary number of dimensions, and so is the $\mathcal{G}_C$ distribution. Therefore, multivariate $\mathcal{G}_C$ distributions could also be considered to exploit the maximum of information from polarimetric data.

V. Amplitude Return

The distribution of the amplitude return that arises from the product of $Z_A = X_A \cdot Y_A$, where $X_A \sim \mathcal{N}^{-1/2}(\alpha,\gamma,\lambda)$ and $Y_A \sim \Gamma^{1/2}(n,n)$ is denoted here as $\mathcal{G}_A(\alpha,\gamma,\lambda,n)$ and is

$$\begin{array}{lll} & \Gamma^{1/2}(\alpha,\lambda) \xrightarrow[\alpha,\lambda\to\infty,\ \alpha/\lambda\to\beta_1]{\Pr} \beta_1^{1/2} & \\ \mathcal{N}^{-1/2}(\alpha,\gamma,\lambda) \xrightarrow[\alpha,\lambda>0]{\gamma\downarrow 0} & \text{Heterogeneous} & \\ \mathcal{N}^{-1/2}(\alpha,\gamma,\lambda) & & \text{Homogeneous,} \\ \mathcal{N}^{-1/2}(\alpha,\gamma,\lambda) \xrightarrow[-\alpha,\gamma>0]{\lambda\downarrow 0} & \text{Extremely heterogeneous} & \\ & \Gamma^{-1/2}(\alpha,\gamma) \xrightarrow[-\alpha,\gamma\to\infty,\ -\alpha/\gamma\to\beta_2]{\Pr} \beta_2^{-1/2} & \end{array} \tag{4}$$

$$\begin{array}{lll} & \mathcal{K}_C(\alpha,\lambda) \xrightarrow[\alpha,\lambda\to\infty,\ \alpha/\lambda\to\beta_1]{\mathcal{D}} \mathcal{N}(0,\beta_1/2). & \\ \mathcal{G}_C(\alpha,\gamma,\lambda) \xrightarrow[\alpha,\lambda>0]{\gamma\downarrow 0} & \text{Heterogeneous} & \\ \mathcal{G}_C(\alpha,\gamma,\lambda) & & \text{Homogeneous,} \\ \mathcal{G}_C(\alpha,\gamma,\lambda) \xrightarrow[-\alpha,\gamma>0]{\lambda\downarrow 0} & \text{Extremely heterogeneous} & \\ & \mathcal{G}_C^0(\alpha,\gamma) \xrightarrow[-\alpha,\gamma\to\infty,\ -\alpha/\gamma\to\beta_2]{\mathcal{D}} \mathcal{N}(0,1/(2\beta_2)). & \end{array} \tag{5}$$

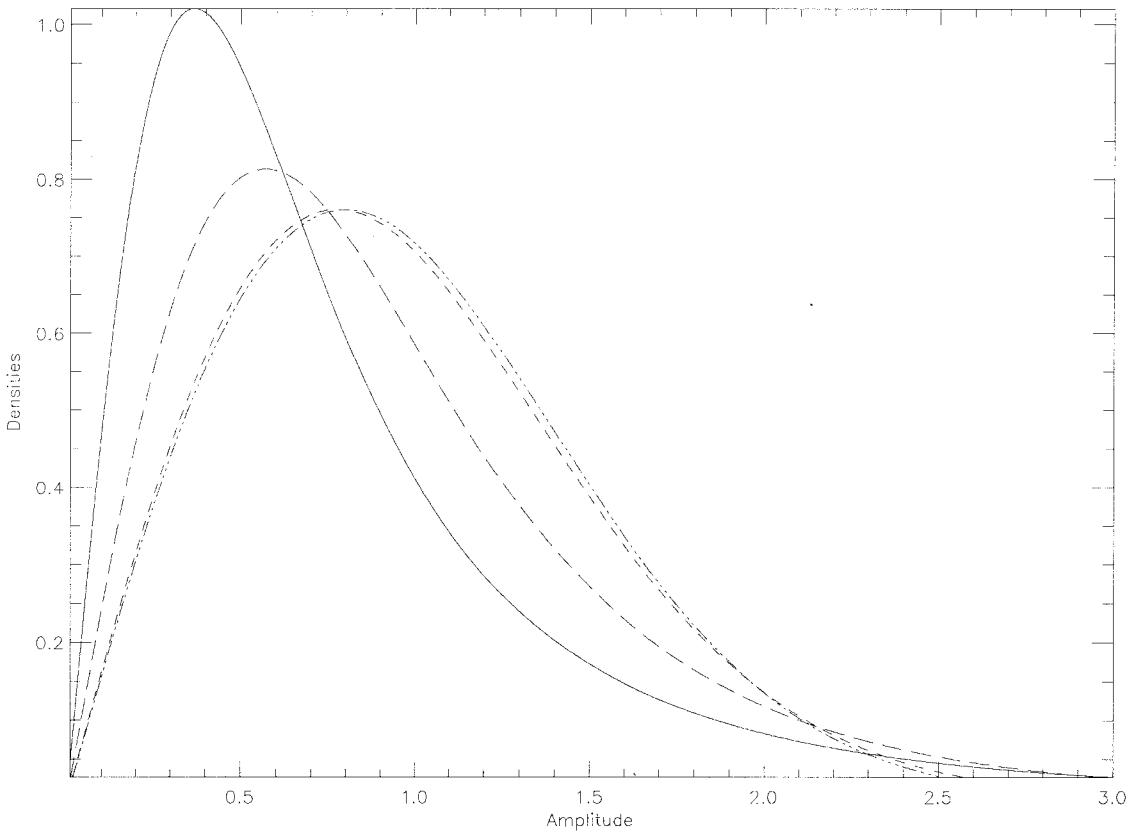

Fig. 1. Densities of the $\mathcal{G}_A^0(-1, 0.405, 1)$ (solid), $\mathcal{G}_A^0(-2, 1.621, 1)$ (long dashes), $\mathcal{G}_A^0(-20, 24.512, 1)$ (dashes) and $\Gamma^{1/2}(1, \pi/4)$ (dash-dot-dot-dot) distributions.

characterized by the density

$$f_{Z_A}(x) = \frac{2n^n(\lambda/\gamma)^{\alpha/2}}{\Gamma(n)K_\alpha(2\sqrt{\lambda\gamma})} x^{2n-1}\left(\frac{\gamma + nx^2}{\lambda}\right)^{(\alpha-n)/2} \times K_{\alpha-n}(2\sqrt{\lambda(\gamma+nx^2)}), \quad x \in \mathbb{R}, \tag{6}$$

and parameters space given in (1). Its rth order moments are given by

$$E(Z_A^r) = \left(\frac{\gamma}{n^2\lambda}\right)^{r/4} \frac{K_{\alpha+r/2}(2\sqrt{\gamma\lambda})\Gamma(n+r/2)}{K_\alpha(2\sqrt{\gamma\lambda})\Gamma(n)}.$$

The relations presented in (4) yield to the properties for the amplitude return presented in (7), shown at the bottom of the next page, where $\mathcal{K}_A$ and $\mathcal{G}_A^0$ denote the amplitude $\mathcal{K}$ and amplitude $\mathcal{G}^0$ distributions, characterized by the following densities

$$f_{Z_A}(x) = \frac{4\lambda n x}{\Gamma(\alpha)\Gamma(n)}(\lambda n x^2)^{(\alpha+n)/2-1} K_{\alpha-n}(2x\sqrt{\lambda n}), \quad \alpha, \lambda, n, x > 0 \tag{8}$$

$$f_{Z_A}(x) = \frac{2n^n\Gamma(n-\alpha)\gamma^{-\alpha}x^{2n-1}}{\Gamma(n)\Gamma(-\alpha)(\gamma+nx^2)^{n-\alpha}}, \quad -\alpha, \gamma, n, x > 0. \tag{9}$$

The r-th order moments of these distributions are given, respectively, by

$$E(Z_A^r) = (n\lambda)^{-r/2}\frac{\Gamma(n+r/2)\Gamma(\alpha+r/2)}{\Gamma(n)\Gamma(\alpha)},$$

$$E(Z_A^r) = (\gamma/n)^{r/2}\frac{\Gamma(-\alpha-r/2)\Gamma(n+r/2)}{\Gamma(-\alpha)\Gamma(n)}$$

In this manner, every amplitude return can be seen as the outcome of a particular case of a $\mathcal{G}_A(\alpha, \gamma, \lambda, n)$ distributed random variable.

Notice that the density given in (9) does not involve Bessel functions making, thus, its evaluation and use simple numerical tasks. It is possible to write the cumulative distribution function of this distribution as

$$F_{Z_A}(x) = \frac{n^{n-1}\Gamma(n-\alpha)x^{2n}}{\gamma^n\Gamma(n)\Gamma(-\alpha)} {}_2F_1(n, n-\alpha; n+1; -nx^2/\gamma), \quad -\alpha, \gamma, n, x > 0$$

where ${}_2F_1$ is the hypergeometric function [6]. A similar distribution, derived as the square root of the ratio of two correlated Gamma random variables, is presented in [11] as a model for multilook amplitude band ratios.

Fig. 1 shows the densities of the $\mathcal{G}_A^0$ distribution for different values of α, γ, with $n = 1$, such that the mean is unitary. The distribution $\Gamma^{1/2}(1, \pi/4)$, shown in dash-dot-dot-dot, represents the limiting case $\alpha = -\infty$, [see relations (7)]. It can be seen from the plot that this last distribution is very close to the $\mathcal{G}_A^0$ with $\alpha = -20$ and, therefore, the $\Gamma^{1/2}$ is a good approximation to the $\mathcal{G}_A^0$ distribution for values of α smaller than about -20. Fig. 2 shows the densities for different values of γ, n, with $\alpha = -1$, such that the mean is unitary, showing the strong effect of the equivalent number of looks on this distribution for low values of the return.

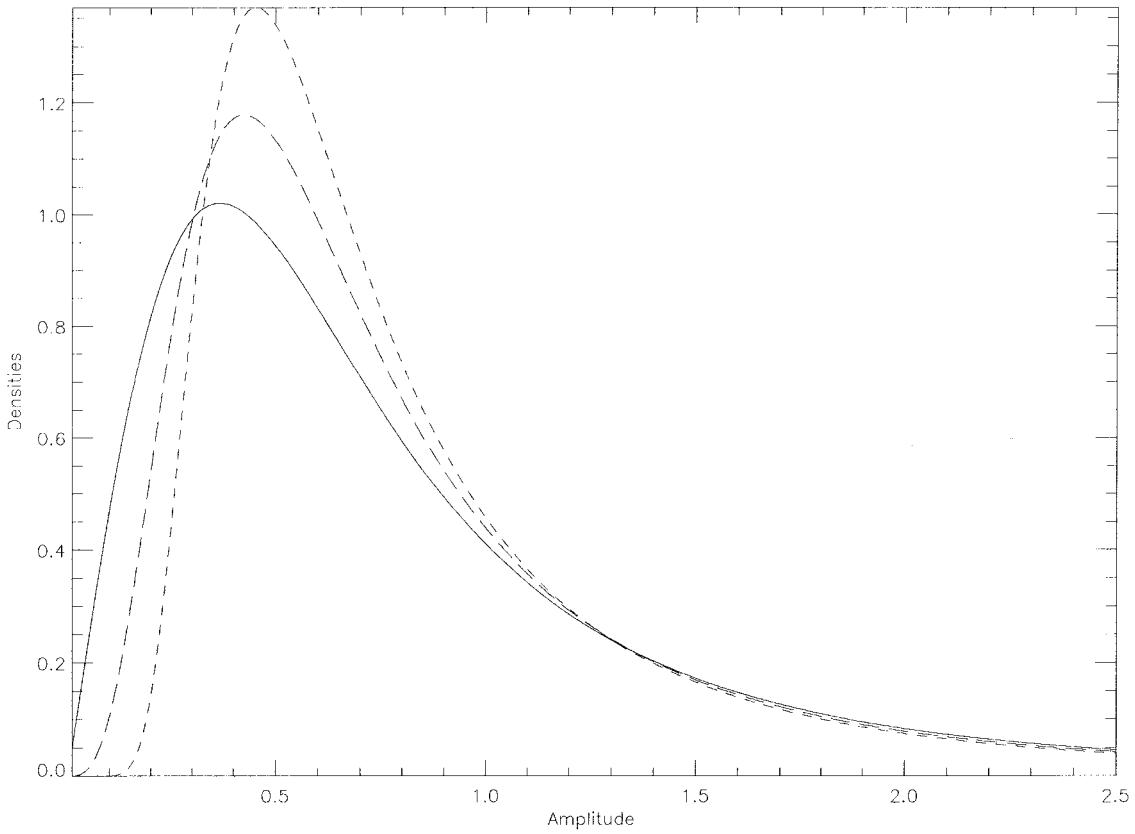

Fig. 2. Densities of the $\mathcal{G}_A^0(-1, 0.405, 1)$ (solid), $\mathcal{G}_A^0(-1, 0.360, 2)$ (long dashes) and $\mathcal{G}_A^0(-1, 0.328, 8)$ (dashes) distributions.

VI. Intensity Return

The distribution of the intensity return is that of the product $Z_I = X_A^2 \cdot Y_I$, which can be obtained from the densities of the amplitude return by the transformation $f_{X_I}(x) = f_{X_A}(\sqrt{x})/(2\sqrt{x})$. Applying this transformation to (6), (8), and (9) one obtains the densities

$$f_{Z_I}(x) = \frac{n^n(\lambda/\gamma)^{\alpha/2}}{\Gamma(n)K_\alpha(2\sqrt{\lambda\gamma})}x^{n-1}\left(\frac{\gamma+nx}{\lambda}\right)^{(\alpha-n)/2} \times K_{\alpha-n}(2\sqrt{\lambda(\gamma+nx)}),$$

$$f_{Z_I}(x) = \frac{2\lambda n}{\Gamma(\alpha)\Gamma(n)}(\lambda n x)^{(\alpha+n)/2-1}K_{\alpha-n}(2\sqrt{\lambda n x}), \quad \alpha, \lambda, n, x > 0,$$

$$f_{Z_I}(x) = \frac{n^n\Gamma(n-\alpha)x^{n-1}}{\gamma^\alpha\Gamma(n)\Gamma(-\alpha)(\gamma+nx)^{n-\alpha}}, \quad -\alpha, \gamma, n, x > 0$$

that characterize the $\mathcal{G}_I$ (with parameters space given in (1)), $\mathcal{K}_I$ and $\mathcal{G}_I^0$ distributions, respectively.

Analogous limiting properties to those presented in (7) can be easily obtained for these distributions. Their rth order moments are given by $E(Z_I^r) = E(Z_A^{2r})$, where $E(Z_A^r)$ is the rth order moment of the corresponding amplitude random variable, which is given in Section V. A closed (recursive) form for the cumulative distribution function of $\mathcal{K}_I$ and $\mathcal{K}_A$ distributed random variables can be found in [19].

VII. Modeling Urban Areas

When estimating the three parameters of the $\mathcal{G}_A$ distribution over urban areas it was always observed that the attractor and global solution of the system of equations was in the parameters space subset given by $(\alpha < 0, \gamma > 0, \lambda < 10^{-6})$;

$$\begin{array}{lll} & \mathcal{K}_A(\alpha,\lambda,n) & \xrightarrow[\substack{\alpha,\lambda\to\infty \\ \alpha/\lambda\to\beta_1}]{\mathcal{D}} \quad \Gamma^{1/2}(n, n/\beta_1) \\ \mathcal{G}_A(\alpha,\gamma,\lambda,n) & \text{Heterogeneous} & \text{Homogeneous}, \\ \text{General Situation} & \text{Extremely heterogeneous} & \\ & \mathcal{G}_A^0(\alpha,\gamma,n) & \xrightarrow[\substack{-\alpha,\gamma\to\infty \\ -\alpha/\gamma\to\beta_2}]{\mathcal{D}} \quad \Gamma^{1/2}(n, n\beta_2). \end{array} \tag{7}$$

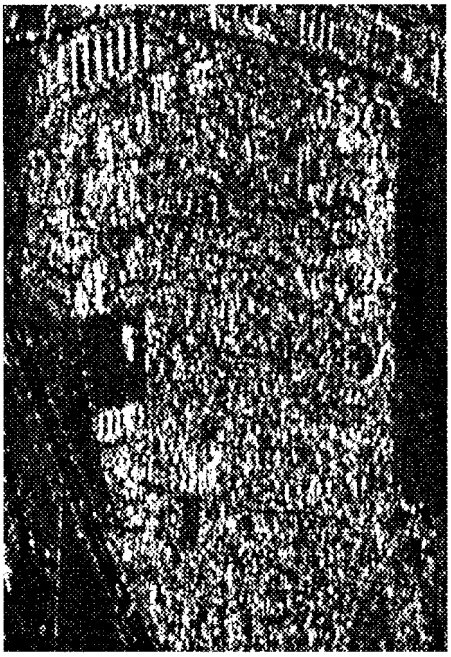

Fig. 3. Gilching urban area, L-HH polarization, 1 look.

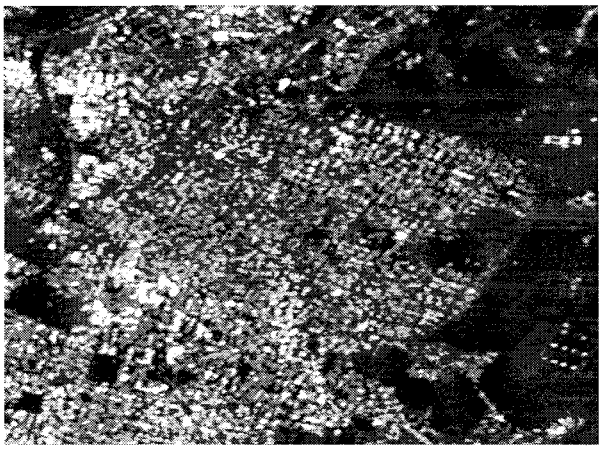

Fig. 4. Weilheim urban area, P-HH polarization, 4 looks.

the $\mathcal{G}_A$ density corresponding to the case $\lambda = 0$ was presented in (9).

Therefore, assuming that the observed values of λ are small enough to allow the use of the $\mathcal{G}_A^0$ distribution, there is empirical evidence that the amplitude return of urban areas can be modeled as having the distribution characterized by the density given in (9).

Using the convergence properties stated in (4), the degree of heterogeneity can be measured with the estimated value of α, i.e., if estimation is performed over two areas and $\hat{\alpha}_1$ and $\hat{\alpha}_2$ are the estimated parameters, then $\hat{\alpha}_1 > \hat{\alpha}_2$ suggests that the first area is more heterogeneous than the second.

Parameter estimation was performed solving the (system of) moment equations. For amplitude data, and assuming n known, the estimators for the parameters of the $\Gamma^{1/2}(n, n/\beta)$, $\mathcal{K}_A(\alpha, \lambda, n)$ and $\mathcal{G}_A^0(\alpha, \gamma, n)$ distributions are

TABLE I
MAIN E-SAR SYSTEM PARAMETERS

RF-Band	X-Band	C Band	L-Band	P Band
Centre Frequency	9.6 GHz	5.3 GHz	1.3 GHz	450 MHz
Wavelength	3.1 cm	5.7 cm	23 cm	67 cm
Transmit Peak Power	2500 W	50 W	360 W	180 W
Receiver Noise Figure	3.5 dB	5.0 dB	8.0 dB	4.5 dB
Antennas	Pyramidal Horn	Microstrip Patch Array	Passive Phased Array	Microstrip Patch Array
Antenna Gain	17.5 dB	17 dB	17 dB	12 dB
Azimuth Beamwidth	17°	19°	18°	30°
Elevation Beamwidth	30°	33°	35°	60°
Polarization	**VV**, HH	VV,**HH**	VV,VH,**HH**	VV,**HH**
Bandwidth	120 MHz	120 MHz	100 MHz	25(60) MHz
Noise equivalent σ°	-30 dB	-25 dB	-35 dB	-35 dB
Pulse Repetition Freq.	1200 Hz	952 Hz	670 Hz	670 Hz
Radiometric Resolution	1 Look: 3 dB and 4 Looks: 1.9 dB			
Sample Frequency	100 or **60** or 20 MHz			

TABLE II
INFORMATION ABOUT THE IMAGES COVERING URBAN AREAS

Location	Gilching			Weilheim
Flight Date	7-21-94	9-28-94	7-21-94	8-24-94
Flight Altitude	3787 m	3774 m	3748 m	3714 m
Incidence Angle	57.4°	57.5°	57.0°	53.0°
Range Resolution	4 m	4 m	4 m	4 m
Azimuth Resolution	3 m	3 m	3 m	3 m 10 m
Range Pixel Spacing	2.5 m	2.5 m	2.5 m	2.5 m
Azimuth Pixel Spacing	2.1 m	1.4 m	1.1 m	1.2 m 4.8 m

given, respectively, by

$$\hat{\beta} = \hat{m}_2;$$

$$\begin{cases} \frac{\Gamma(n)\Gamma(n+1/2)\Gamma(\hat{\alpha})\Gamma(\hat{\alpha}+1/2)}{(\Gamma(n+1/4)\Gamma(\hat{\alpha}+1/4))^2} - \frac{\hat{m}_1}{\hat{m}_{1/2}^2} = 0 \\ \hat{\lambda} = \left(\frac{\Gamma(n+1/2)\Gamma(\hat{\alpha}+1/2)}{\Gamma(n)\Gamma(\hat{\alpha})\hat{m}_1}\right)^2 \frac{1}{n} \end{cases}$$

$$\begin{cases} \frac{\Gamma^2(-\hat{\alpha}-1/4)\Gamma^2(n+1/4)}{\Gamma(-\hat{\alpha}-1/2)\Gamma(n+1/2)\Gamma(-\hat{\alpha})\Gamma(n)} - \frac{\hat{m}_{1/2}^2}{\hat{m}_1} = 0 \\ \hat{\gamma} = n\left(\frac{\hat{m}_1\Gamma(-\hat{\alpha})\Gamma(n)}{\Gamma(-\hat{\alpha}-1/2)\Gamma(n+1/2)}\right)^2, \end{cases}$$

where $\hat{m}_j$ denotes the jth order sample moment. The estimators for the parameters of the two last distributions were derived using $r = 1/2, 1$.

The SAR data used for modeling urban areas were acquired by the DLR's airborne Experimental SAR system (E-SAR), developed and built by its Institute of High Frequency [7]. E-SAR is mounted on board of a Dornier DO 228 aircraft. It currently operates in X-, C-, L- and P-bands with vertical or horizontal polarization, except L-band which works fully polarimetric. Special features are small fixed antennas with a wide azimuth beam permitting high azimuth resolution and motion error compensation in the off-line SAR image processor. Table I summarizes the technical key parameters of E-SAR system, while Table II presents information specific to the images covering the selected urban area.

From E-SAR data takes two urban areas were selected, Gilching (48°5′35″N, 11°12′54″E) and Weilheim (47°56′2″N, 11°5′9″E). These are small towns to the west and to the south

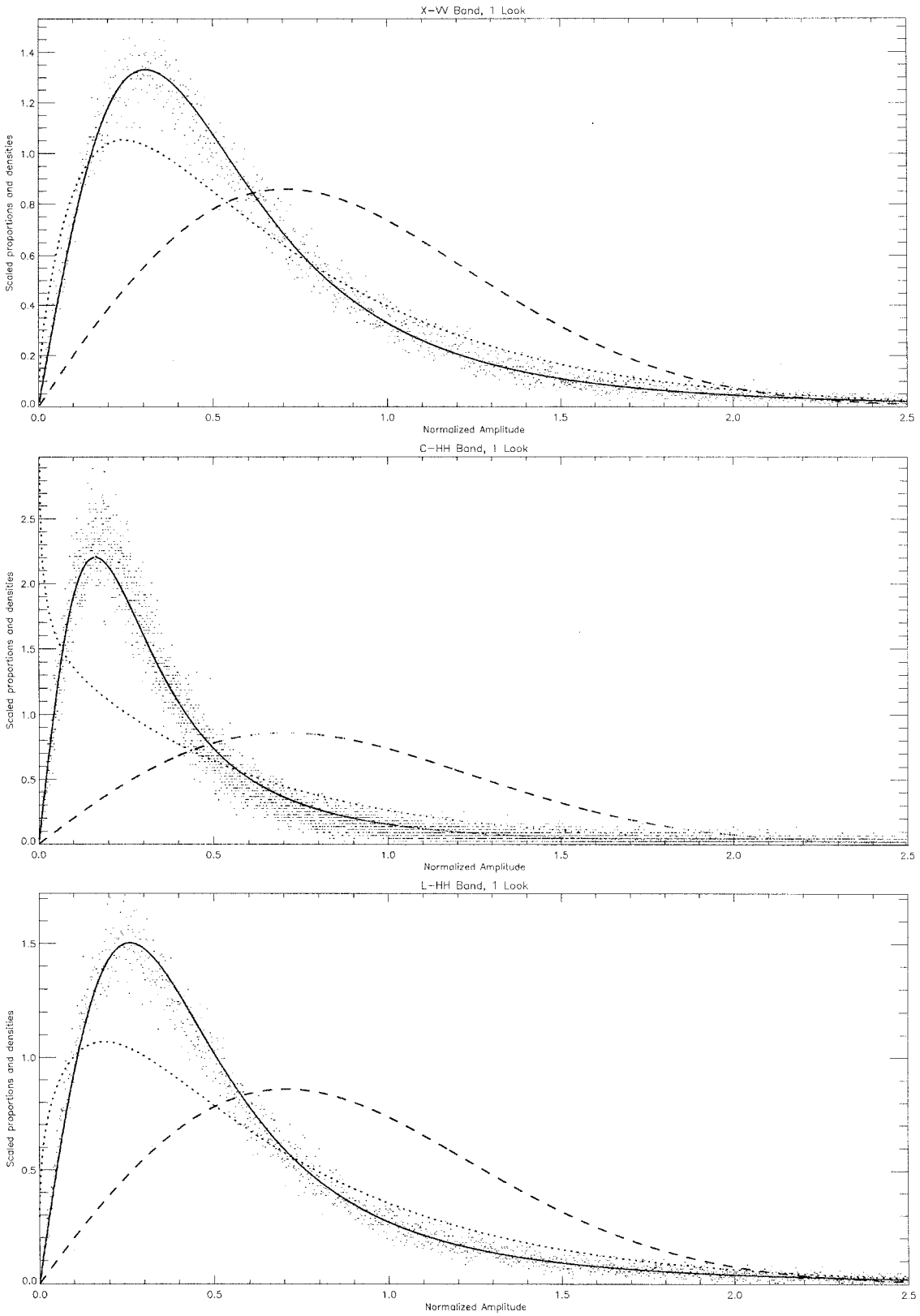

Fig. 5. Histogram and estimated densities of Gilching urban area: $\Gamma^{1/2}$ (dashes), $\mathcal{K}_A$ (dots) and $\mathcal{G}_A^0$ (continuous lines, resp).

of the Bavarian capital, Munich. The E-SAR image data are in amplitude format and slant range. They are calibrated, and they do not have to be further corrected by elevation and slope because these urban areas are located on flat terrain.

These two urban areas were described with the $\Gamma^{1/2}$, $\mathcal{K}_A$ and $\mathcal{G}_A^0$ distributions. The sample sizes of the Gilching data (1 look amplitude) were 232 $\times$ 368 (X-VV band), 228 $\times$ 364 (C-HH band) and 248 $\times$ 432 (L-HH band) pixels. The

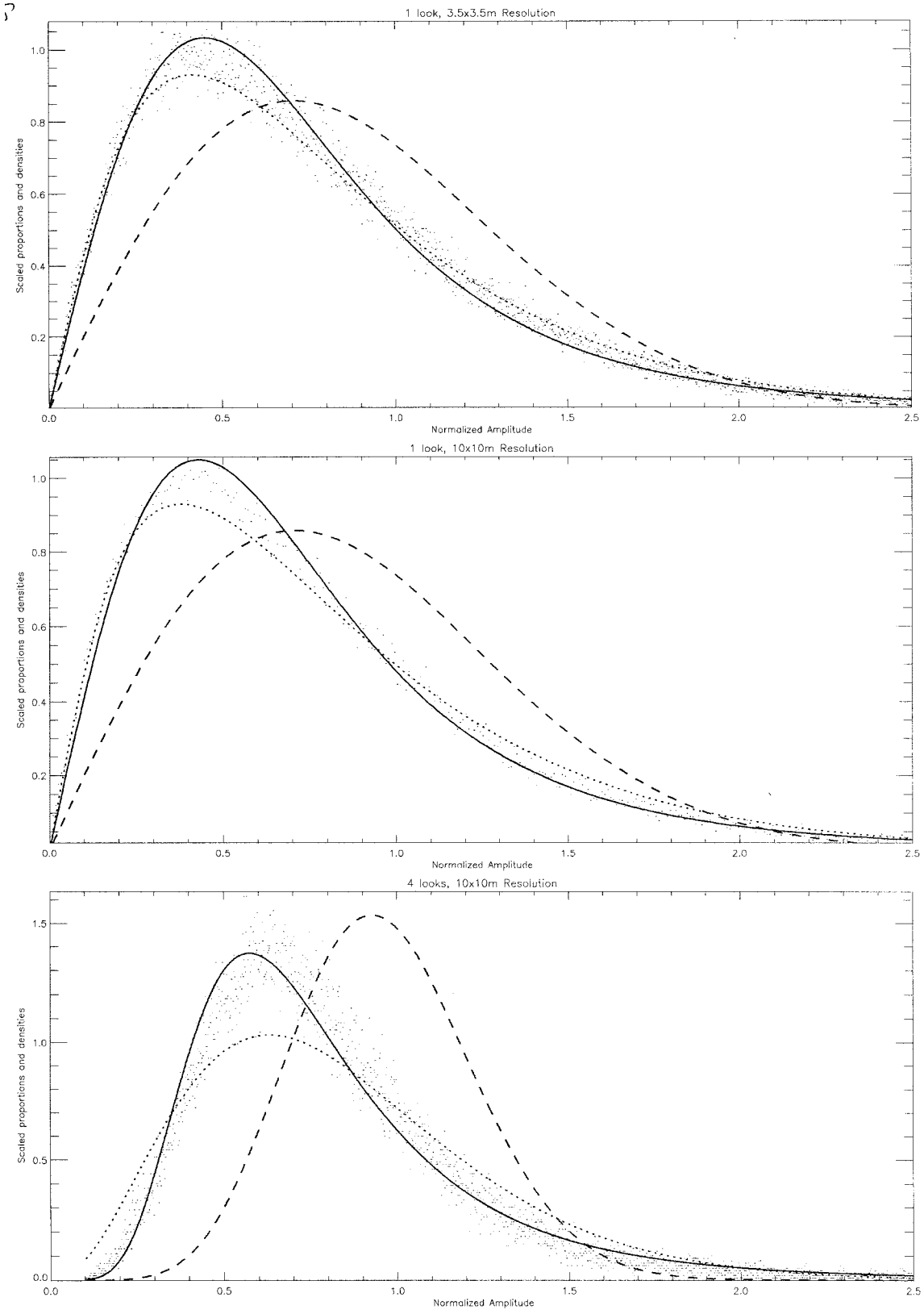

Fig. 6. Histogram and estimated densities of Weilheim urban area: $\Gamma^{1/2}$ (dashes), $\mathcal{K}_A$ (dots) and $\mathcal{G}_A^0$ (continuous lines, resp).

sample sizes of the Weilheim P-HH band data were 268 $\times$ 720 (1 look, 3 m azimuth resolution), 268 $\times$ 300 (1 look, 10 m) and 328 $\times$ 196 (4 looks, 10 m) pixels, respectively. For this last image, an equivalent number of looks $n = 3{,}6$ was estimated and used in the forthcoming analysis. Fig. 3 shows the Gilching area and its surroundings in the L-HH band; Fig. 4 shows the P-HH band, 4 looks image over Weilheim and its surroundings.

TABLE III
ANALYSIS OF GILCHING DATA, 1 LOOK, DIFFERENT POLARIZATIONS

Band	$\widehat{CV}$	$\hat{\beta}$	$(\hat{\alpha},\hat{\lambda})$	$(\hat{\alpha},\hat{\gamma})$	p_{χ^2}
X-VV	1.093	282498	$(0.791, 3.576 \cdot 10^{-6})$	$(-1.292, 96074.4)$	0.34
C-HH	1.709	3572790	$(0.397, 1.979 \cdot 10^{-7})$	$(-0.897, 266363)$	0.22
L-HH	1.225	407589	$(0.632, 2.105 \cdot 10^{-6})$	$(-1.131, 90636.6)$	0.62

TABLE IV
ANALYSIS OF WEILHEIM DATA, 1 AND 4 LOOKS, SAME POLARIZATION

Looks / Resol.	$\widehat{CV}$	$\hat{\beta}$	$(\hat{\alpha},\hat{\lambda})$	$(\hat{\alpha},\hat{\gamma})$	p_{χ^2}
1 / 3.5m	0.790	255911	$(1.547, 6.577 \cdot 10^{-6})$	$(-2.048, 264945)$	0.29
1 / 10m	0.785	146232000	$(1.308, 9.418 \cdot 10^{-9})$	$(-1.807, 124839000)$	0.07
4 / 10m	0.658	415658	$(1.516, 4.148 \cdot 10^{-6})$	$(-2.018, 401329)$	0.14

Before doing the goodness-of-fit tests the data were subsampled in a 1 to 16 ratio (only one pixel every 4×4 window was considered), in order to reduce the effect of spatial correlation on the test statistics. Parameters estimation was performed using the whole datasets to obtain more accurate values. The results of the analysis are shown in Tables III and IV, where the first column identifies the data, the second shows the estimated coefficient of variation ($\widehat{CV}$), while the next three present the estimated parameters of the aforementioned distributions. The last column shows the p-value of the χ^2 goodness-of-fit test of the $\mathcal{G}_A^0$ distribution. Fitting the other two distributions always produced $p_{\chi^2} = 0$, with the only exception being the $\mathcal{K}_A$ distribution for the first Weilheim data set, that produced $p_{\chi^2} = 0.06$.

Table III shows the results of the analysis of Gilching data, and Fig. 5 shows the histogram of the whole set of data and the estimated densities. From this table and this figure it can be concluded that both $\Gamma^{1/2}$ and $\mathcal{K}_A$ give very poor statistical description of the data, whilst $\mathcal{G}_A^0$ is a good model. Table IV shows the results of the analysis of Weilheim data, and Fig. 6 shows the histogram of the whole set of data and the estimated densities. It is evident, again, the feasibility of the use of the $\mathcal{G}_A^0$ distribution for urban areas modeling, against the inadequacy of the other two distributions.

The observed inadequacy of the $\mathcal{K}_A$ distribution for these data is in accordance with the results presented in [12], where it is shown that data for which $\widehat{CV} > 0.75$ is not well fitted by this distribution. One look urban data was also fitted with the Nakagami-Rice distribution [5]. The estimated parameters led to the $\Gamma^{1/2}$ distribution, which is a particular case of the Nakagami-Rice model.

VIII. MODELING PRIMARY FOREST AND DEFORESTED AREAS

As presented in relations (7), the $\mathcal{G}_A^0(\alpha,\gamma,n)$ distribution has the capability of modeling a continuously varying degree of homogeneity, being $\alpha \to -\infty$ the extreme homogeneous situation where this distribution is equivalent to a $\Gamma^{1/2}(n, n/\beta_2)$ distribution (scaled speckle). In this section the fitting of the previously presented distributions is shown for primary forest and deforested areas, with varying degrees of homogeneity. It is shown that the $\mathcal{G}_A^0$ distribution is a good model for these areas, and that the deforested area (more homogeneous) is also well fitted by the $\Gamma^{1/2}$ distribution, as expected from relations (7).

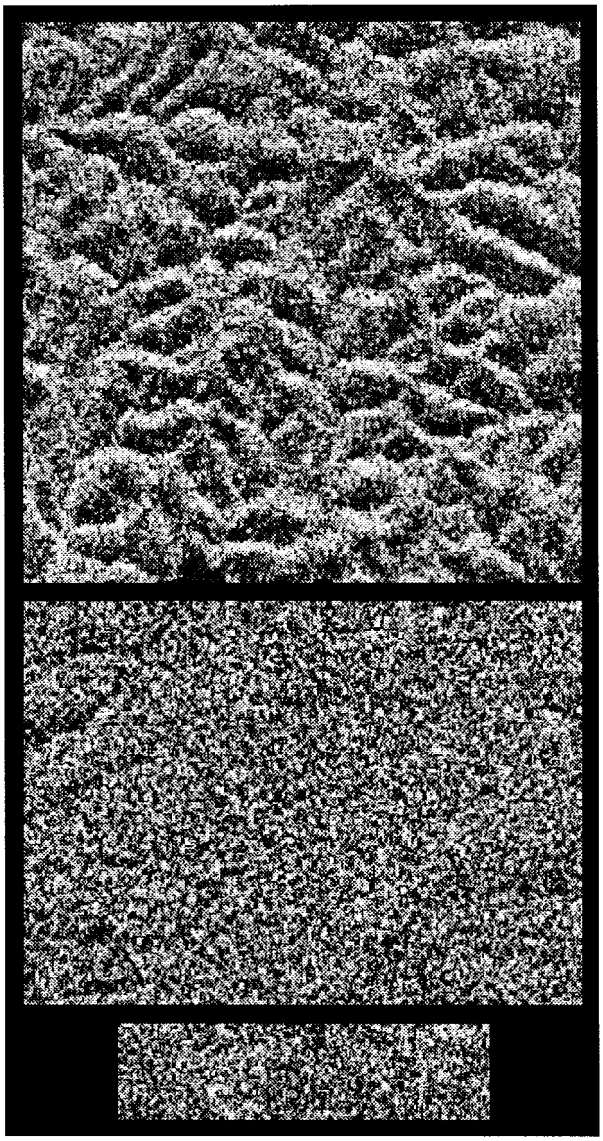

Fig. 7. JERS-1 samples: primary forest with undulated relief, primary forest with flat relief and deforestation, from top to bottom.

TABLE V
ANALYSIS OF JERS-1 DATA

Sample	$\widehat{CV}$	$\hat{\beta}$	$(\hat{\alpha},\hat{\lambda})$	$(\hat{\alpha},\hat{\gamma})$	p_{χ^2} $\Gamma^{1/2}$	$\mathcal{K}_A$	$\mathcal{G}_A^0$
Und. relief	0.463	1361240	$(2.254, 1.877 \cdot 10^{-6})$	$(-3.040, 2819050)$	0.00	0.01	0.04
Flat	0.335	1303020	$(13.652, 1.048 \cdot 10^{-5})$	$(-14.290, 17314500)$	$5 \cdot 10^{-4}$	0.78	0.81
Defor.	0.318	684111	$(21.157, 3.083 \cdot 10^{-5})$	$(-21.657, 14180400)$	0.69	0.84	0.48

The image used for this part of the study was taken on June 26, 1993 over Tapajós, Pará, Brazil, by JERS-1. The main parameters of the instrument are L-HH band (wavelength of 24 cm), spatial resolution of 18 m, nominal look angle of 35 degrees and three looks (nominal). The estimated number of looks, used in the forthcoming statistical modeling, was of 2.84 [17].

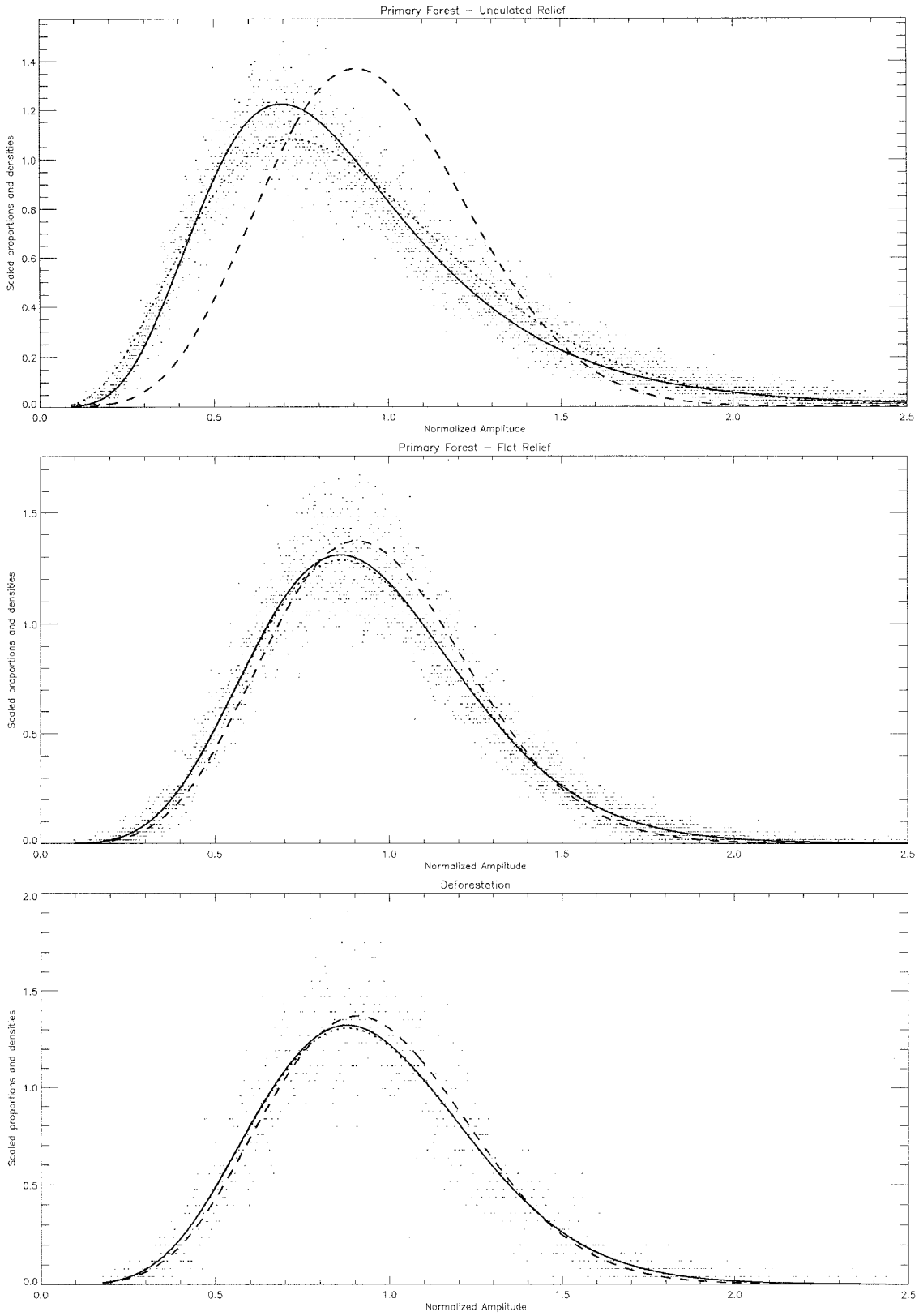

Fig. 8. Histogram and estimated densities of JERS-1 samples: $\Gamma^{1/2}$ (dashes), $\mathcal{K}_A$ (dots) and $\mathcal{G}_A^0$ (continuous lines, resp).

Three samples were taken from this image, two from different types of primary forest and one from a deforested area. The two primary forests differ with respect to their relief (one is undulated while the other is relatively flat) and with respect to their vegetation types, among other factors. Fig. 7 shows these three samples; their sizes are, respectively, of 300 $\times$ 300, 300 $\times$ 216, and 200 $\times$ 52 pixels. Table V shows the estimated parameters and the p_{χ^2} values obtained with the

same methodology described in Section VII. Fig. 8 presents the histograms of the whole data sets and the estimated densities.

From the plots and the estimates of α it can be observed that, as expected, this parameter is strongly related to the degree of homogeneity of the data, being smaller for more homogeneous areas such as the deforested one. Also, as $\hat{\alpha}$ decreases the fit with the $\Gamma^{1/2}$ distribution becomes better and all the three densities tend to be alike; note that for deforested data it was observed $p_{\chi^2} = 0.69$ when fitting the $\Gamma^{1/2}$ distribution.

IX. Conclusion

Some useful distributions for SAR image modeling and analysis for several degrees of heterogeneity and usual image formats were derived within the multiplicative model. Many relationships between these distributions were presented. An extension of "classic" distributions that arise within the multiplicative model is given through the use of the square root of generalized inverse Gaussian distribution for the amplitude backscatter, giving rise to the class of $\mathcal{G}$ distributions for the return. A two-parameters particular case of the amplitude $\mathcal{G}$ distribution, called here $\mathcal{G}_A^0$, is presented in this paper.

The modeling improvement of the $\mathcal{G}_A^0$ distribution, with respect to the $\mathcal{K}_A$ distribution, becomes evident when fitting urban, forested, and deforested areas, with widely varying degrees of homogeneity.

Efficient estimation techniques for the $\mathcal{G}_C(\alpha, \gamma, \lambda)$, $\mathcal{G}_A(\alpha, \gamma, \lambda, n)$ and $\mathcal{G}_I(\alpha, \gamma, \lambda, n)$ distributions is a problem currently under study.

Acknowledgment

The authors are grateful to O. E. Barndorff-Nielsen (Århus University, Denmark) and O. H. Bustos (FaMAF, Argentina) who made substantial contributions to this work. The authors also would like to thank FAPESP, PROTEM-CC/CNPq, the GEOTEC Project, and Dr. J. Moreira (DLR) and Dr. L. V. Dutra (INPE).

References

[1] O. E. Barndorff-Nielsen and P. Blæsild, "Hyperbolic distributions and ramifications: Contributions to theory and applications," *Statistical Distributions in Scientific Work*, C. Taillie and B. A. Baldessari, Eds. Dordrecht, Germany: Reidel, 1981, pp. 19–44.

[2] R. G. Caves, "Automatic matching of features in synthetic aperture radar to digital map data," Ph.D. Thesis, University of Sheffield, Sheffield, UK, 1993.

[3] A. C. Frery, C. C. F. Yanasse, and S. J. S. Sant'Anna, "Alternative distributions for the multiplicative model in SAR images," in *Quantitative Remote Sens. Sci. Applicat., Int. Geosci. Remote Sensing Symp.*, Florence, Italy, July 10–14, 1995, vol. 1, pp. 169–171.

[4] ——, "Statistical characterization of SAR data: The multiplicative model and extensions," *Simposio Latinoamericano de Especialistas en Percepción Remota (SELPER)*. Mexico, Nov. 1995, pp. 502–515.

[5] J. W. Goodman, "Statistical properties of laser speckle patterns," *Laser Speckle and Related Phenomena*, J. C. Dainty, Ed. New York: Springer-Verlag, 1984, ch. 2.

[6] I. S. Gradshteyn and I. M. Ryzhik, *Table of Integrals, Series and Products: Corrected and Enlarged Edition*. New York: Academic, 1980.

[7] R. Horn, "DLR airborne SAR project, objectives and status," in *Proc. 1 Int. Airborne Rem. Sens. Conf. Exhibit.*, Strasbourg, France, 1994.

[8] E. Jakeman and P. N. Pusey, "A model for non-Rayleigh sea echo," *IEEE Trans. Antennas Propagat.*, vol. AP-24, pp. 806–814, 1976.

[9] J. K. Jao, "Amplitude distribution of composite terrain radar clutter and the K distribution," *IEEE Trans. Antennas Propagat.*, vol. AP-32, pp. 1049–1061, 1984.

[10] B. Jørgensen, *Statistical Properties of the Generalized Inverse Gaussian Distribution*, New York: Springer-Verlag, 1982, Lecture Notes in Statistics, 9.

[11] J. S. Lee, K. W. Hoppel, S. A. Mango, and A. R. Miller, "Intensity and phase statistics of multilook polarimetric and interferometric SAR imagery," *IEEE Trans. Geosci. Remote Sensing*, vol. 32, pp. 1017–1027, 1994.

[12] A. Lopes, H. Laur, and E. Nezry, "Statistical distribution and texture in multilook and complex SAR images," in *Remote Sensing Science for the Nineties, International Geoscience and Remote Sensing Symposium,* Washington, DC, May 20–24, 1990, vol. 3, pp. 2427–2430.

[13] H.-J. Müller, "Backscatter stastistics from terrain with airborne DLR E-SAR data," in *Proc. PIERS'94*, Noordwijk, The Netherlands, 1994.

[14] C. J. Oliver, "Information from SAR images," *J. Phys. D: Appl. Phys.*, vol. 24, pp. 1493–1514, 1991.

[15] M. Tur, K. C. Chin, and J. W. Goodman, "When is speckle noise multiplicative?" *Appl. Opt.*, vol. 21, pp. 1157–1159, 1982.

[16] F. T. Ulaby, F. Kouyate, B. Brisco, and T. M. Williams, "Textural information in SAR images," *IEEE Trans. Geosci. Remote Sensing*, vol. GRS-24, pp. 235–245, 1986.

[17] P. R. Vieira, "Maximum likelihood and ICM SAR image classifiers," *M.Sc. Thesis, INPE*, Brazil, 1996 (in Portuguese).

[18] C. C. F. Yanasse, A. C. Frery, S. J. S. Sant'Anna, P. H. Filho, and L. V. Dutra, "Statistical analysis of SAREX data over Tapajós—Brazil," in *Workshop Proceedings*, SAREX-92 South American Radar Experiment, Paris, Dec. 6–8, 1993, pp. 25–40, 1994.

[19] C. C. F. Yanasse, A. C. Frery, and S. J. S. Sant'Anna, *Stochastic Distributions and the Multiplicative Model: Relations, Properties, Estimators and Applications to SAR Image Analysis*, INPE, São José dos Campos, Brazil, 1995, INPE-5630-NTC/318.

Alejandro César Frery (M'91) was born in Mendoza, Argentina, in 1960. He received the engineering degree in electronics and electricity from the Universidad de Mendoza in 1985, the M.Sc. degree in applied mathematics (statistics) from the Instituto de Matemática Pura e Aplicada (IMPA), Rio de Janeiro, Brazil, in 1990, and the Ph.D. degree in computer science from the Instituto Nacional de Pesquisas Espaciais, São José dos Campos, Brazil, in 1993.

He is currently with the Computer Science Department, Universidade Federal de Pernambuco, Recife, Brazil. His activities focus on the development and the use of statistical techniques (Markov random fields, inference, robustness, simulation, etc.) applied to image synthesis, processing, and analysis.

Häns-Jürgen Müller received the Diploma Physiker in theoretical and experimental physics from the University of Munich, Germany, in 1967.

Coming from the fields of crystallography and thin layers in X-ray and vacuum technique, he worked in cloud physics, artificial influenced rain, fog control, and forming of ice nuclei at the Institute for Atmospheric Research. He was responsible for the deep space antenna station of the HELIOS probe, the national German ship station, and the two frequency scatterometer for measuring ocean waves. He belonged to the science group pushing forward the German draft of the process language PEARL by applying it in the simulated workplace for Spacelab experiments. In the early 1990's, he was the responsible scientist for data evaluation of the Shuttle/Spacelab experiment MRSE. Since then he was more and more involved in microwave remote sensing at the Institute for Radio Frequency, DLR. Presently, he is aircraft operator of the airborne ESAR system and member of the Geomatic group at DLR interpretating SAR images with emphasis to statistics and forest problems.

Corina da Costa Freitas Yanasse was born in São Paulo, Brazil, in 1952. She received the B.S. degree in mathematics from the Pontifícia Universidade Católica de São Paulo in 1974, the M.Sc. degree in statistics from the Massachusetts Institute of Technology, Cambridge, in 1980, and the Ph.D. degree in statistics from the University of Sheffield, UK, in 1992.

She is currently a Researcher at the Instituto Nacional de Pesquisas Espaciais (INPE), São José dos Campos, Brazil. Her research interests include statistical analysis of SAR images and SAR image formation.

Sidnei João Siqueira Sant'Anna was born in Rio de Janeiro, Brazil, in 1965. He received the degree of engineer electronics and electricity from the Universidade Federal do Rio de Janeiro in 1993, the M.Sc. degree from the Instituto Nacional de Pesquisas Espaciais (INPE), São José dos Campos, Brazil in the area of remote sensing in 1995.

He is currently a Consultant at INPE, and his interests are image analysis and processing techniques for remote sensing (SAR image filtering, statistical methods, robustness, etc.).